Transcutaneous Magnet Localizer for a Self-Contained Myokinetic Prosthetic Hand

Valerio Ianniciello, Marta Gherardini, and Christian Cipriani, *Senior Member, IEEE*

***Abstract*—*Objective*: The search for a physiologically appropriate interface for the control of dexterous hand prostheses is an ongoing challenge in bioengineering. In this context, we proposed an interface, named *myokinetic control interface*, based on the localization of magnets implanted in the residual limb muscles, to monitor their contractions and send appropriate commands to the artificial hand. As part of such concept, this interface requires a transcutaneous magnet localizer that can be integrated in a self-contained limb prosthesis, a feature yet to be realized within the current state of the art. *Methods:* In an attempt to cover this gap, here we present a modular embedded system consisting of a computation unit able to acquire synchronized samples captured by up to eight acquisition units, so to localize multiple magnets. *Results:* The system exhibits short computation times (<60ms) and power consumption (0.6-1.2W) which are suitable for use in a clinically viable prosthetic arm. The system proved able to localize magnets while moving at speeds in the range of physiological movements (<0.24m/s), with high accuracy (<1mm) and precision (<0.5mm). *Conclusion:* We demonstrated a system suitable for the implementation of a self-contained myokinetic prosthetic hand. *Significance:* These results pave the way towards the clinical implementation of the myokinetic interface, with amputees controlling an artificial arm by means of implanted magnets.**

***Index Terms*—Embedded control system, magnetic tracking, myokinetic control interface, prosthetic control.**

I. Introduction

MAGNETIC tracking/localization has attracted the interest of biomedical engineering researchers for its prospective use in a variety of applications, such as tracking of catheters, needle tips or endoscopic capsules during surgical or diagnostic procedures [1], [2].

Indeed, as the human body is transparent to low-frequency magnetic fields [1], such fields represent an ideal solution for monitoring/inspecting or acting remotely on different organs or body districts, even for long-term applications [3], [4], [5], [6].

Manuscript received 22 May 2023; revised 31 August 2023; accepted 16 October 2023. Date of publication 19 October 2023; date of current version 26 February 2024. This work was supported by European Research Council through MYKI Project ERC-2015-StG, under Grant 679820. *(Corresponding author: Christian Cipriani.)*

Valerio Ianniciello and Marta Gherardini are with the BioRobotics Institute and the Department of Excellence in Robotics and AI, Italy.

Christian Cipriani is with the BioRobotics Institute and the Department of Excellence in Robotics and AI, Scuola Superiore Sant'Anna, 56127 Pisa, Italy (e-mail: christian.cipriani@santannapisa.it).

Digital Object Identifier 10.1109/TBME.2023.3325910

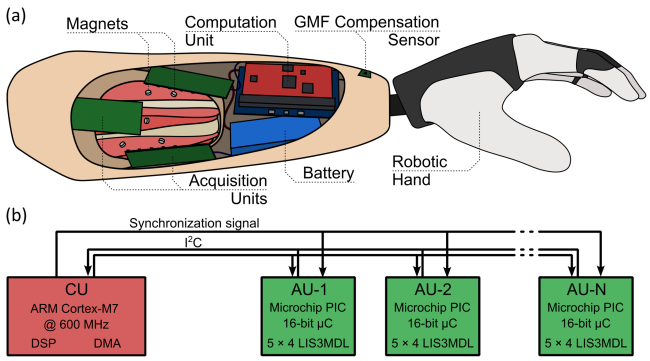

Fig. 1. Overview of the myokinetic control interface for a transradial prosthetic hand. Magnets are implanted in relevant residual muscles; the voluntary contractions of these muscles are monitored by the transcutaneous magnet localizer–TML (details in the lower panel), which use these signals to control the physiologically appropriate movements in the artificial hand. The transcutaneous localizer includes up to eight acquisition units (AUs), each including 20 magnetic field sensors, an additional sensor placed far from the magnets to compensate for the geomagnetic field (GMF), and an ARM M7-based computation Unit (CU), that localizes the magnets.

In this context, we recently proposed a novel human-machine-interface for the control of upper limb prostheses, based on magnetic tracking and dubbed it the *myokinetic control interface* [7]. Such an interface deploys permanent magnets implanted in the residual limb muscles, in order to decipher the individual's motor intentions, by tracking displacements of the magnets caused by muscle contractions. This approach was first proposed to treat transradial amputations, by targeting and taking advantage of the extrinsic muscles of the hand which are anatomically associated to the hand and wrist and thus could entail dexterous biomimetic control [7] (Fig. 1(a)). The myokinetic interface fits into a landscape of innovative surgical procedures and technologies aimed at restoring a more natural control in prosthetic limbs [8], [9], [10], [11]. Among these we cite the neuromusculoskeletal interface [9], which exploits epymisial electrodes wired through percutaneous titanium implants to probe the electromyography (EMG) signal from the muscles. Another example is that of wireless implantable myoelectric sensors, first proposed by Reilly in 1970 [12] and later reintroduced by Weir in 2009 under the name IMES [10]. IMES can be inserted inside the muscles belly through a small surgery and can wirelessly transmit the acquired EMG signal to an external controller, exploiting a transcutaneous magnetic link. Compared to these or similar solutions, a major advantage brought by the myokinetic interface is the use of passive implants, which eliminates the need for power supply,

percutaneous wires, electrical maintenance, as well as the risk of electrical failures.

More in detail, the myokinetic control interface comprises of multiple magnets implanted in independent muscles, and a Transcutaneous Magnet Localizer (TML) integrated in the prosthetic socket and ideally constrained to the stump, so that no relative movements are possible. The TML is responsible for continuously localizing/tracking the pose of the magnets (namely their position and orientation in space) so to ultimately send control commands to the prosthetic limb (Fig. 1(a)). It may be composed of acquisition units (AUs), hosting magnetic field sensors which sample the field generated by the implanted magnets, and a computation unit (CU) to localize them. Localization may be achieved by either exploiting modelling [7], [13], [14], [15] or machine learning approaches [16].

In the last years, the concept of the myokinetic interface has gained interest in the scientific community, as demonstrated by a number of scientific publications and projects deploying this idea [17], [18], [19]. Of particular interest is the study by Moradi et al. [19], who demonstrated the clinical viability of the approach in a transradial amputee by implanting three magnets in the flexor muscles and implementing a basic online controller (one magnet and one sensor). Taylor et al. [18], [20] also contributed to the concept of a myokinetic interface and demonstrated in vivo tissue length measurements in a Turkey's gastrocnemius. They used two custom AUs and a personal computer as CU for localizing the magnets online [18], akin to Biancalana and colleagues [21]. Prakash et al. [17] proposed a non-invasive version of the myokinetic interface which uses a Hall sensor and a disc magnet mechanically coupled through a spring to capture muscular contraction from the skin surface. However, none of the aforementioned studies have developed a system that seamlessly integrates into a self-contained prosthesis.

Integrating the complete system within the prosthetic socket represents an essential step for the clinical deployment of the myokinetic control interface. To this aim, the system not only needs to be miniaturized, energy-efficient, and operate in real-time, but also demands sub-millimetric precision to ensure nuanced proportional control across multiple tiers, and a bandwidth able to capture the entirety of movements falling within the physiological range. A prerequisite for this is a dedicated technical effort to design a custom hardware architecture, entailing true portability. Earlier we described a fully embedded system including 32 three-axes magnetic field sensors arranged on a single AU, and a microprocessor-based CU, enabling the localization of up to five magnets [22]. The system demonstrated highly accurate and precise (sub-millimeter precision), yet exhibiting very short computation times (4ms for five magnets). Nevertheless, the analysis of the temporal scheduling clearly revealed the architecture of the AU to be the bottleneck of the system; the overall output rate was indeed tied to the number of sensors and in that case restrained to $\sim$29ms for a fixed number of 32 sensors, allowing in that spatial configuration to localize up to five magnets. In addition, sampling across sensors could not be synchronized due to hardware limitations, and this affected the consistency of the acquired samples and in turn the bandwidth of the localizer (namely, the maximum speed of *localizable* magnets). Finally, as the geomagnetic field was not compensated for, it affected localization performance, curtailing its deployment.

Here we present a novel architecture aimed at addressing the limits of previous implementations and suitable for integration in self-contained limb prostheses (Fig. 1(a)). Specifically, we designed a modular and parallel architecture able to capture synchronized samples from one AU (100Hz sampling frequency) to up to eight AUs (38Hz sampling frequency), with geomagnetic field compensation. The system proved light enough for integration in a self-contained prosthesis (30g for the CU, 8g for each AU) and capable to operate through a standard prosthetic battery; its power consumption ranged from $<$600mW with one AU to $\sim$1.2W for eight AUs.

We used an anatomical forearm mockup containing up to eight magnets to generate experimental data mimicking those that would be present in a clinical implant. Using this data, we proved the feasibility of localizing up to eight simultaneously moving magnets with an output rate lower than 60ms, and remarkable accuracy. Furthermore, we showed that the localization accuracy was not affected by the dynamics of muscle contractions, in the physiological range.

Taken together, these outcomes pave the way towards the clinical deployment of a new class of voluntarily controlled prosthetic or assistive devices, exploiting implanted magnets.

II. Architecture of the Transcutaneous Magnet Localizer

The TML includes AUs (up to eight), each hosting 20 magnetic field sensors, one geomagnetic field compensation sensor and a microprocessor-based CU (Fig. 1). The architecture is modular, meaning that its hardware and firmware allow to use and assemble a variable number of AUs, to be adapted to different clinical cases and number of implanted magnets. The AUs sample synchronously, meaning that readings from 20 to 160 sensors occur all at the same time instant, thus ensuring consistent measurements. Through a 1.7MHz dedicated bus (I^2C), the AUs sequentially transfer the samples to the CU, which are thus fetched by the localization algorithm to retrieve the poses, at each cycle, of potentially up to 80 magnets, considering that the localization of a single magnet requires theoretically only two sensors. The localization algorithm operates in pipeline (concurrently) with the AU sampling and AUs-CU data transferring (Fig. 2).

More in detail, the AUs are based on custom boards each mounting 20 three-axis magnetic field sensors (LIS3MDL, STMicroelectronics, Geneva, Switzerland), arranged on a 4×5 grid with a 9mm inter-sensor distance. These sensors exhibit a 16-bit output resolution, selectable full-scale values ($\pm$4G, $\pm$8G, $\pm$12G, and $\pm$16G), and communicate via a serial bus with a 16-bit low power microcontroller (PIC24F, Microchip Technology Inc., Chandler, AZ), solely responsible for sampling synchronization and transfer. The full-scale value of each sensor can be adjusted independently based on the magnitude of the field sensed in previous acquisitions, so to obtain optimal sensitivity (while avoiding saturation). However, this feature has

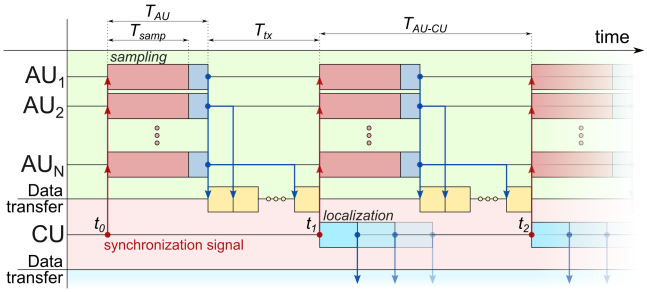

Fig. 2. Temporal diagram of the tasks involved in the localizer. The magnetic field is sampled synchronously across all the acquisition units (AU) in response to a synchronization signal (red arrow) issued by the computation unit (CU). The field is digitized (red rectangle) in a fixed time, T_{samp} (6.6 ms), made available to the AU microcontroller (blue rectangle) within T_{AU} (8.2 ms), and transferred from the AUs to the CU (yellow rectangles) with a 2.2 ms transfer time for each AU (T_{tx} = N_{AU}·2.2 ms). $T_{AU\text{-}CU}$ refers to the lag between two consecutive synchronization signals. The localization algorithm (azure rectangle) fed with the sample at time t_{i-1}, runs concurrently with the sampling and transferring of the sample at time t_i. The localized poses of the magnets can be used for control of the limb prosthesis.

not been utilized in the tests keeping the sensors at the highest full-scale, to maintain sensor acquisitions independent of their history, thus enhancing data repeatability. The TML includes an additional sensor, to be placed far from the implanted magnets, that senses the geomagnetic field and serves for compensating it through differential measurements, as in [7], [22], [23], [24].

The CU, based on the i.MX RT1060 Real Time Processor running on an Arm Cortex-M7 core at 600 MHz (Fig. 1(b)), implements the localization algorithm. The latter derives the poses of N magnets by modelling the field at the i^{th} sensor, B_i, as a linear superposition of that produced by N magnetic dipoles [25]:

$$\boldsymbol{B_i} = \sum_{j=1}^{N} \frac{\boldsymbol{M_j \mu_r \mu_0}}{4\pi} \left(\frac{3\,(\widehat{\boldsymbol{m_j}} \cdot \boldsymbol{x_{ij}})\,\boldsymbol{x_{ij}}}{|\boldsymbol{x_{ij}}|^5} - \frac{\widehat{\boldsymbol{m_j}}}{|\boldsymbol{x_{ij}}|^3} \right) \tag{1}$$

Where M_j and m_j are the magnitude and the direction of the magnetic moment of the j^{th} magnet, respectively, and x_{ij} is the unknown vector distance between the i^{th} sensor and the j^{th} magnet. A number of equations equal or higher than 6 N (viz. a number of three-axis sensors $\geq 2N$) is needed to solve the inverse problem (so called *inverse problem of magnetostatics*) and thus to retrieve the unknown poses. However, as there is no closed form solution for this, a numerical approximation is needed, and the Levenberg-Marquardt algorithm (LMA) proved an effective choice [22], [26]. The localization algorithm runs the LMA for each new data package received from the AUs, and converges to a solution when the squared differences between the acquired and estimated fields is less than machine precision square root. The result is considered acceptable only if the magnets are localized within a user defined workspace, which in our case corresponds to the internal volume of a forearm. Otherwise, the localization is marked as incorrect and the LMA is re-run until an acceptable solution is found. The CU implements custom code optimizations exploiting the DSP (digital signal processing) and DMA (direct memory access) capabilities of the Cortex-M7, for reducing the computation time of the localization.

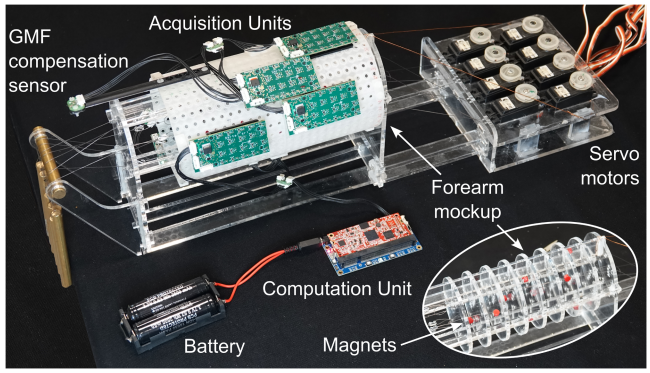

Fig. 3. Experimental setup used for the localization of Individual and simultaneous movements. An anatomical mockup of the forearm, with muscles linearly actuated via servo motors, emulates individual and simultaneous muscle contractions. Up to eight magnets (Table I) and acquisition units were used. Bottom right insert: Placement of the magnets in the mockup.

Samples over multiple AUs are synchronized via a dedicated signal issued by the CU and synchronously repeated by each AU to all 20 sensors (Fig. 2). The magnetic field is then sampled in parallel (conversion time $T_{samp} = 6.6$ ms) and sequentially transferred to the AU microcontroller, sensor by sensor (within $T_{AU} = 8.2$ ms). Each packet is then sequentially transferred from the AUs to the CU with a 2.2 ms transfer time for each AU. Hence, the AU-CU rate, defined as the interval of time at which complete data packages are transmitted to the CU increases with the number of acquisition units (N_{au}), according to:

$$T_{AU-CU} \approx 2.2 \cdot N_{AU} + 8.2 \ \text{(ms)} \tag{2}$$

As the CU runs the LMA concurrently with the sampling and transferring of the new packet, $T_{AU\text{-}CU}$ coincides with the output rate of the whole system, unless the LMA takes more time than $T_{AU\text{-}CU}$.

III. Experimental Validation

A. Localization of Individual Movements

We built a mockup of the human forearm to simulate magnet implantation, using wires to mimic the anatomical position and orientation of the muscles, and servo motors to pull the wires and mimic contraction, as in [7], [22], [25] (Fig. 3). Eight modeled muscles were selected as targets to mimic the implant, namely: (i) flexor digitorum superficialis, (ii) extensor digitorum, (iii) flexor carpi radialis, (iv) extensor carpi radialis longus, (v) abductor pollicis longus, (vi) flexor pollicis longus, (vii) flexor carpi ulnaris, (viii) extensor carpi ulnaris. Eight configurations including one to eight magnets (modeled muscles) were considered in these validation tests for the TML (Table I). A number of AUs matching the number of magnets in each configuration was used, resulting in a number of sensors ranging from 20 (one magnet, one AU) to 160 (eight magnets, eight AUs). To ensure accurate localization, magnets and AUs were arranged in space following two guidelines: i) the *R rule*, which requires that the ratio between the inter-magnet distance and the magnet-to-sensor distance is above a specified value (*R*

TABLE I
EXPERIMENTAL CONFIGURATIONS USING THE FOREARM MOCKUP

Configuration / No. of magnets	Mockup modeled muscles with a magnet attached
1	Flexor digitorum superficialis (FDS)
2	Conf. #1 + Extensor digitorum (ED)
3	Conf. #2 + Flexor carpi radialis (FCR)
4	Conf. #3 + Extensor carpi radialis longus (ECRL)
5	Conf. #4 + Abductor pollicis longus (APL)
6	Conf. #5 + Flexor pollicis longus (FPL)
7	Conf. #6 + Flexor carpi ulnaris (FCU)
8	Conf. #7 + Extensor carpi ulnaris (ECU)

≥ 0.6) [27]; ii) the use of one AU for each magnet to place it in the optimal position for the localization of that magnet.

For each configuration, one magnet at a time was displaced without rotating along a trajectory of 10mm discretized into 200μm steps while keeping the other magnets steady in their rest position. Five static acquisitions were made at each step and used to assess the localization accuracy and precision. The localization error E is defined as the difference between the estimated displacement/rotation D_{est} and the actual one D_{act}. When magnets are moving one at a time, E at a certain instant can be described as:

$$E = D_{est} - D_{act} \approx e_m + \sum_{j=1}^{n-1} e_{ct_j} \quad (3)$$

where e_m is the model error and e_{ct} the cross-talk error [7], [22]. Notably, e_m accounts for inaccuracies in retrieving the movement of the moving magnet, while e_{ct} refers to false predictions of simultaneous movements detected for the steady ones. Both those errors are computed for the position (e_{m_p}, e_{ct_p}) and the orientation (e_{m_o}, e_{ct_o}) and are reported as the 95th percentile of the measures. Localization precision S, and specifically the different components S_{m_p}, S_{ct_p}, S_{m_o} and S_{ct_o}, were derived as the 95th percentile of the standard deviation of the corresponding error obtained at each step [22], [25].

B. Localization of Simultaneous Movements

The performance of the TML were assessed also in the case of simultaneous movements of multiple magnets, considering the same eight configurations used in the previous batch of tests. Specifically, we used the servo motors to apply sinusoidal movements to each magnet (10mm fixed amplitude; frequency randomly assigned in the range 0.5-1Hz). The minimum $T_{AU\text{-}CU}$ for each configuration was used, according to (2), and multiple cycles ($\geq$15) were acquired for each magnet and configuration.

As the acquisition and the magnets motion frequencies are not multiples of each other, it became necessary to interpolate the positions of the magnets as localized by the TML to derive equidistant steps for each sinusoidal cycle, thus enabling the analysis of variability within each bin. Windows of 0.1 ms per step were considered. Since it was not possible to distinguish between model and cross-talk errors, we derived the overall localization accuracy E_p as the 95th percentile of the difference between the estimated and actual displacements across all steps and cycle. The precision, S_p, was instead computed as the 95th percentile of the standard deviation of the localization error derived at each step, across different cycle. The orientation error was not assessed as the actual rotation of the magnets could not be properly controlled and measured along the trajectory.

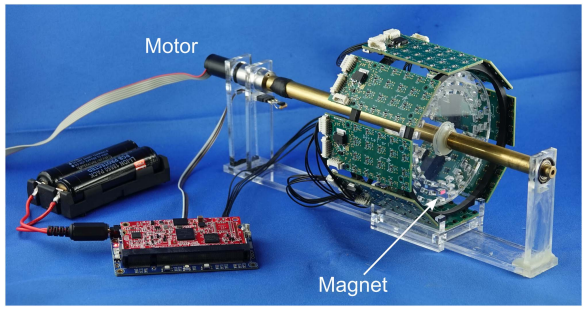

Fig. 4. Experimental setup used for the characterization of the bandwidth. Eight acquisition units (AUs) and the computation unit (CU) sample and localize one magnet placed on a plexiglass disc and rotated by a motor at different speeds.

C. Computation Time

The computation time of the LMA is not predictable a-priori, since the number of iterations needed to converge to a solution depends on the unknown configuration of the magnets in space [25], [28]. Thus, the computation time was measured through the CU internal clock for all the eight configurations, and for both individual and simultaneous movement conditions.

D. Bandwidth

The bandwidth of the TML was characterized by localizing a single magnet while moving at different speeds. More in detail, the magnet, placed in a circular frame and pointing radially, was rotated by an electric motor and monitored by eight AUs arranged around the frame at 20mm radial distance from it (Fig. 4). The tangential velocity of the magnet was varied between 0.1–0.6m/s (equivalent to a rotation frequency of the motor of 0.6–3.1Hz): a range including muscle dynamics of both average people and professional piano players [29], [30]. At each revolution the localization was triggered and for each velocity 85 rotations/measurements were completed.

IV. RESULTS

A. Localization of Individual Movements

e_{m_p} and e_{m_o} reached their maximum values at 1.32mm and 18.73°, respectively, for the magnet attached to the APL in the five-magnets configuration (Fig. 5). In terms of position, this corresponded to $\sim$13% the entire trajectory travelled by the magnet. The error variability associated to the same magnet proved equal to 0.07mm and 0.33° (S_{m_p} and S_{m_o}, respectively). A maximum e_{m_p} (e_{m_o}) of 0.79 mm (12.35°), associated with an S_{m_p} (S_{m_o}) of <0.01 mm (0.06°), was found for the remaining magnets and all configurations.

The greatest cross-talk error was found for the magnet implanted in FPL, in the seven-magnets configuration, with an

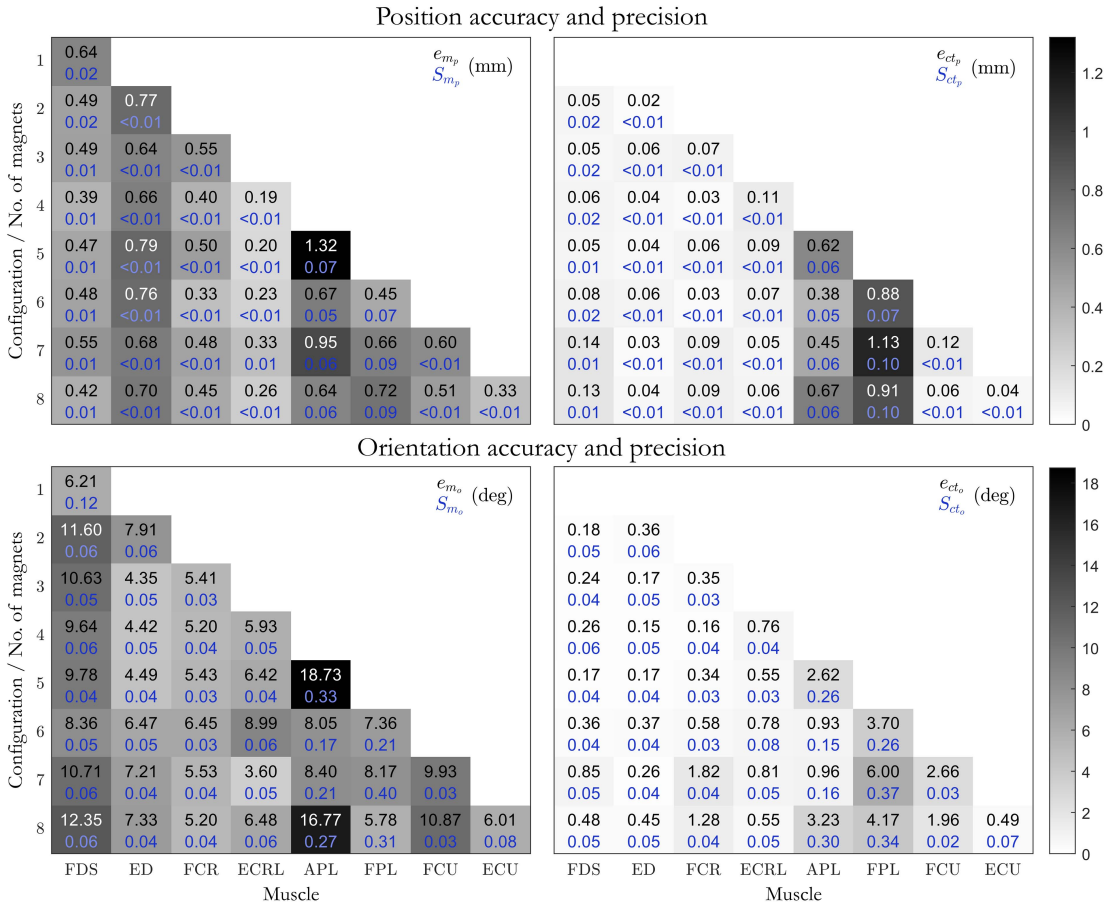

Fig. 5. TML accuracy and precision with individual movements. Position errors (e_{m_p}, e_{ct_p}) and precision (S_{m_p}, S_{ct_p}) (upper panel), orientation errors (e_{m_p}, e_{m_o}) and precision (S_{m_o}, S_{ct_o}) (lower panel) in localizing independently moving magnets. Each value in black (or in blue) represents the localization error (or precision) for that magnet in a given configuration.

TABLE II
MINIMUM *R* FOR EACH MAGNET IN THE EIGHT-MAGNET CONFIGURATION

Modeled muscle	min (*R*)
FDS	1.68
ED	2.96
FCR	2.36
ECRL	1.78
APL	1.13
FPL	0.87
FCU	2.57
ECU	2.18

e_{ct_p} (S_{ct_p}) of 1.13mm (0.10mm), and an e_{ct_o} (S_{ct_o}) of 6.00° (0.37°). This corresponded to ∼11% the length of the magnet trajectory. For the other magnets and configurations, a maximum e_{ct_p} (e_{ct_o}) of 0.67mm (3.23°), associated with an S_{ct_p} (S_{ct_o}) of 0.06mm (0.30°), was found.

Not surprisingly, the magnets that yielded the worst accuracy and precision (APL and FPL) exhibited the lowest *R* values (1.13 and 0.87, respectively) (Table II).

B. Localization of Simultaneous Movements

The TML proved able to localize up to eight magnets moving simultaneously at different frequencies (Fig. 6). As for localizing

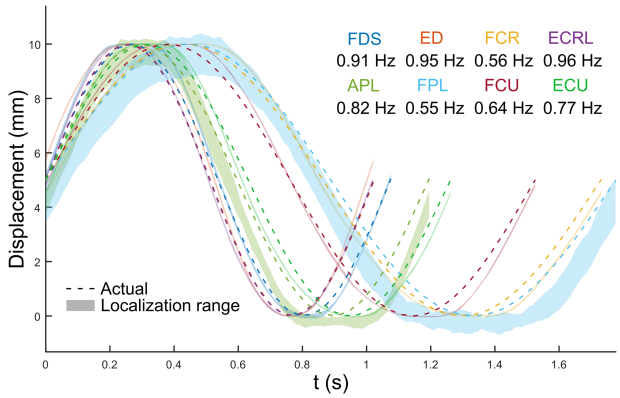

Fig. 6. Simultaneous movements – representative result. Localized displacement of eight magnets moving sinusoidally at different speeds (frequencies in the legend), using eight AUs. The interquartile range of the localization is superimposed (shaded area) for comparison with the actual displacement (dashed line).

independent movements, the magnets fixed on the APL and FPL were the worst localized, with the latter showing maximum values of E_p and S_p of 2.60mm (equal to 26% its stroke), and 1.37mm, respectively (Fig. 7). For the remaining six magnets, E_p and S_p proved always below 0.81mm (corresponding to ∼8%

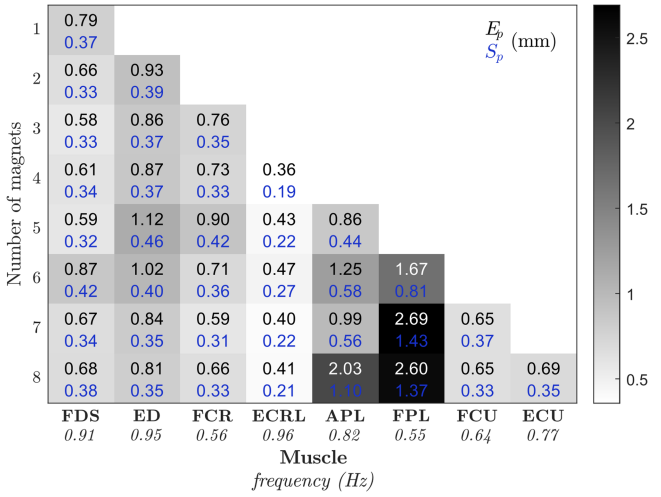

Fig. 7. TML accuracy and precision with simultaneous movements. Position errors (e_{m_p}, e_{ct_p}) and precision (S_{m_p}, S_{ct_p}) in localizing simultaneously moving magnets. Each value in black (or in blue) represents the localization error (or precision) for that magnet in a given configuration.

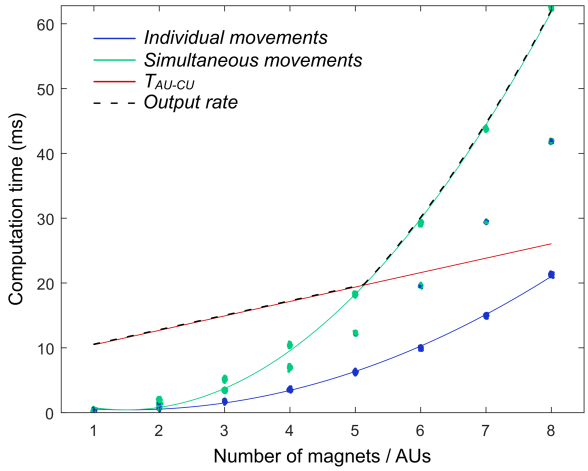

Fig. 8. TML computation time. Computation time for one up to eight magnets, for both individual movements (in blue) and simultaneous movements (in green). $T_{AU\text{-}CU}$ (red line) is superimposed on the graph to depict the fastest output rate (dotted line), which is capped by both $T_{AU\text{-}CU}$ and the computation time of the localization algorithm.

the stroke), and 0.38mm, respectively. The relationship between the actual and the computed displacement proved highly linear for all magnets ($R^2 > 0.95$, $p < 0.001$).

These results generalized well to all the other configurations. The magnets in APL and FPL generally displayed higher localization errors compared to the other magnets, reaching a maximum E_p (S_p) of 1.25mm (0.58mm) and of 2.69mm (1.43mm) in the six- and seven-magnets configuration, respectively (Fig. 7). For the remaining six magnets, E_p proved always below 1.12mm (corresponding to ∼11% the stroke), while S_p proved lower than 0.46mm. As for individual movements, the accuracy proved correlated with the *R* value exhibited by each magnet along its trajectory (Table II). Expanding on this, we found that for magnets associated to higher *R* values (namely, all but those in APL and FPL), we could discriminate >25 discrete steps along the 10mm magnet stroke. Nevertheless, a good precision (∼14% the magnet stroke) was also obtained for APL and FPL, meaning that the localization proved at least repeatable.

We found that higher frequencies of movement did not lead to higher localization errors (not shown). As an example, for the eight-magnets configuration, the one in ECRL moved at ∼1Hz (the highest frequency applied) and showed a maximum E_p (S_p) of 0.47mm (0.27mm), corresponding to ∼5% the trajectory length. The magnet in FPL moving at 0.55Hz (the lowest one), showed a maximum E_p (S_p) of 2.69mm (1.43mm), corresponding to ∼27% the length of the trajectory. Overall, the model and cross-talk error trends obtained across magnets and configurations closely matched those found in the localization of individual movements (Figs. 5 and 7).

C. Computation Time

The computation time of the localization algorithm increased with the number of magnets/AUs and when passing from individual to simultaneous movements (Fig. 8). Specifically, when increasing the number of magnets/AUs, the median computation time quadratically increased ($R^2 > 99\%$) (Fig. 8, blue curve). This increase was associated to a longer duration of each iteration of the LMA, due to a larger system of equation (1): ranging, e.g., from 153μs (one magnet/AU) to 21.3 ms (eight-magnets/AUs). Switching from individual to simultaneous movements, instead, had a clear effect on the number of iterations needed for the LMA to converge (Fig. 8, green curve). The localization time is always an integer multiple of the single iteration time, as evident from the clusters in Fig. 8. The number of iterations needed for convergence of the LMA proved almost constant with magnets/AUs: one or two iterations for localizing independent movements, one to three for simultaneous movements.

The actual output rate of the system (Fig. 8, dashed curve) proved thus limited by the AU-CU channel ($T_{AU\text{-}CU}$) (Fig. 8, red curve) to up to five magnets/AUs, and by the number of iterations required by the LMA to converge, from six to eight magnets/AUs.

D. Bandwidth

The accuracy in estimating the magnet position proved mostly constant, with errors below 70μm, up to a tangential velocity of 0.24m/s (Fig. 9). Notably, this value, roughly proportional to a 4Hz movement on a 2cm displacement (distance calculated basing on the natural range of motion of joints [31] applied to anthropometric data of healthy subjects [32]), falls just behind the dynamics of average people physiological movements [29]. The errors increased quadratically ($R^2 > 90\%$) for higher speeds, albeit proving always below 230μm.

V. Discussion

We presented a new architecture, its associated prototype and the experimental assessment of an embedded, battery operated, transcutaneous magnet localizer suitable for integration in a self-contained myokinetic prosthesis. The system proved able to localize up to eight magnets accurately and promptly, in all tested conditions. Hence, as localizing multiple magnets translates into

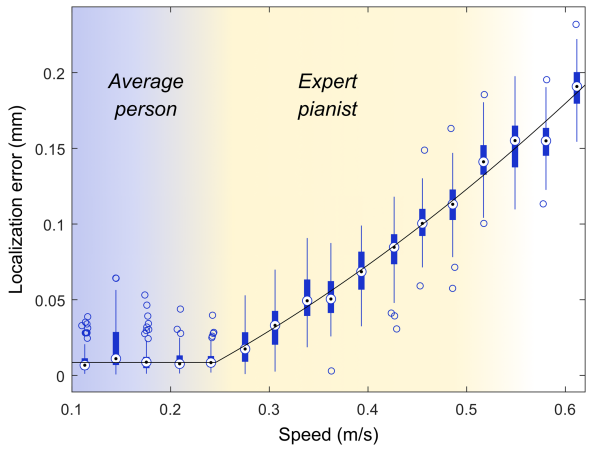

Fig. 9. TML bandwidth. Localization error as a function of magnet's movement speed. Accuracy is constant up to 0.24m/s, then it increases quadratically ($R^2 > 90\%$).

monitoring the contraction of multiple muscles, this technology could enable the control of dexterous hand prostheses, under myokinetic control. In addition, the demonstrated precision enables a fine and graded control of the prosthetic movements. Finally, as the modular architecture allows to arrange in space a variable number of AUs, the system holds the potential to be readily adapted to different clinical conditions.

The experimental measurements (re)confirmed our early findings to up to eight magnets, namely, that a proper magnet placement guarantees an accurate localization regardless the number of magnets, and their kind of movements (individual vs. simultaneous) (Table II, Figs. 5 and 7) [27], [33]. More in detail, the results confirmed that above a certain R value (i.e., magnets positioned close enough to the AUs and/or far enough from the other magnets) [27] the localization decreases significantly [7]. Nonetheless, the overall accuracy proved worse than in previous studies, where errors proved always lower than 1mm with $R \geq 0.6$ [27], [33], [34]. This deterioration, which has shifted the R threshold between 1.13 and 1.68 (Table II, Figs. 5 and 7), was likely caused by the complexities brought in by a physical system, difficult to model in our simulation works.

While suboptimal placements (i.e., lower R value) resulted in lower accuracy, fairly precise localizations ($S_p < 1.5$mm) – precision is the relevant metric for determining the performance of a myokinetic controller [7] – were consistently obtained. Excellent precisions ($S_p < 0.5$mm) were found for the magnets with greatest R (Table II, Figs. 5 and 7). Notably, the lowest accuracy obtained for the two magnets with lowest R values, was achieved when considering the worst-case scenario of simultaneous movements and by computing the error rather conservatively (95^{th} percentile across the whole acquisition).

In this regard, we showed that the speed of muscle contraction, in the range of physiological movements, does not affect the localization accuracy obtained with the present TML (Fig. 9). The quadratic increase in localization error for speeds above 0.24m/s (Fig. 9) is likely ascribed to the non-instantaneous acquisition time needed by the sensors to sample the field (i.e., 6.6 ms). Very likely, for speeds above 0.24m/s, the assumption that the magnetic field is constant in such time window no longer holds true.

The orientation error, reported only for the independent movements, proved relatively high considering that no rotation was actually applied (by design) to the magnets (Fig. 6). This discrepancy is explained by the following. The physical mockup introduces inevitable limitations in the positioning of the magnets. While servomotors can achieve precise magnet movements with an accuracy of $<4\mu$m, other factors that can potentially compromise the exact positioning of the magnets come into play. These factors include minor torsions and frictions experienced by the wires in the mockup, as well as the mutual attraction between the magnets (Fig. 3). While it is reasonable to believe that the impact of these factors on magnet positioning accuracy is minimal compared to the precision of the localizer, the same cannot be said for magnet orientation. During testing, we observed slight twisting of the magnets along their intended trajectories. These deviations, though relatively small, could account for a portion of the orientation error observed. This factor proved even more relevant during simultaneous movements, when all magnets were displaced together; hence we decided not to include these mostly noisy results. In an actual implant, we expect that the magnets would displace and rotate, and that this combined information could indeed increase the quality of the localization [35]. In this view, the correct implementation of the myokinetic control interface would require an appropriate mapping, not only of the magnets displacements, but also of their rotations along with muscle contractions to derive the desired control signals [34].

The proposed system could be further optimized. Firstly, the time needed for localizing multiple magnets proved suitable for controlling a prosthesis, being largely below the acceptable delay perceived by a user [36], [37]. However, the localization time could be further reduced, e.g., by selecting an optimal subset of sensors and thus reducing the system of equations [34]. Secondly, power consumption was considerably reduced compared to our earlier prototype [22], which required $\sim$1W when using one AU (32 sensors). The current TML would require the same amount of power when using five AUs (100 sensors). To give an example: a system with three AUs would require $\sim$13Wh for 16 hours of continuous use, that could be provided by commercially available Li-Ion battery weighting less than 50g [38]. Nevertheless, energy-saving strategies should be further investigated, to make the system a viable alternative to state-of-the art advanced interfaces and controllers [39], [40]. Interestingly, the power consumption of the TML is comparable to that of second generation IMES (implantable myoelectric sensors) [41].

VI. Conclusion

The proposed self-contained TML is capable of accurately localizing multiple moving magnets in real-time. This makes the system well-suited for monitoring the contraction of multiple muscles, enabling the direct, independent and parallel control over multiple degrees of freedom of a dexterous robotic hand. Although further improvements could be made, the current TML solution satisfies all the requirements in terms of localization

error and bandwidth, and is thus suitable for the clinical implementation of the myokinetic interface, wherein individuals with limb loss can control an artificial arm by means of implanted magnets.

REFERENCES

[1] A. M. Franz et al., "Electromagnetic tracking in medicine-A review of technology, validation, and applications," *IEEE Trans. Med. Imag.*, vol. 33, no. 8, pp. 1702–1725, Aug. 2014, doi: 10.1109/TMI.2014.2321777.

[2] F. Bianchi et al., "Localization strategies for robotic endoscopic capsules: A review," *Expert Rev. Med. Devices*, vol. 16, no. 5, pp. 381–403, May 2019, doi: 10.1080/17434440.2019.1608182.

[3] Y. Liao et al., "Magnetically controlled artificial urinary sphincter: An overview from existing devices to future developments," *Artif. Organs*, vol. 47, no. 7, pp. 1075–1093, Jul. 2023, doi: 10.1111/AOR.14535.

[4] E. D. Young and D. Oertel, *Cochlear Nucleus*. London, U.K.: Oxford Univ. Press, 2004, doi: 10.1093/ACPROF:OSO/9780195159561.003.0004.

[5] P. Nachev et al., "Magnetic oculomotor prosthetics for acquired nystagmus," *Ophthalmology*, vol. 124, no. 10, pp. 1556–1564, Oct. 2017, doi: 10.1016/J.OPHTHA.2017.05.028.

[6] A. Villamarin et al., "A new adjustable glaucoma drainage device," *Invest. Ophthalmol. Vis. Sci.*, vol. 55, no. 3, pp. 1848–1852, Mar. 2014, doi: 10.1167/IOVS.13-12626.

[7] S. Tarantino et al., "The myokinetic control interface: Tracking implanted magnets as a means for prosthetic control," *Sci. Rep.*, vol. 7, no. 1, Dec. 2017, Art. no. 17149, doi: 10.1038/s41598-017-17464-1.

[8] T. A. Kuiken et al., "The use of targeted muscle reinnervation for improved myoelectric prosthesis control in a bilateral shoulder disarticulation amputee," *Prosthetics Orthotics Int.*, vol. 28, no. 3, pp. 245–253, 2004, doi: 10.3109/03093640409167756.

[9] M. Ortiz-Catalan, B. Håkansson, and R. Brånemark, "An osseointegrated human-machine gateway for long-term sensory feedback and motor control of artificial limbs," *Sci. Transl. Med.*, vol. 6, no. 257, 2014, Art. no. 257re6, doi: 10.1126/scitranslmed.3008933.

[10] R. F. Weir et al., "Implantable myoelectric sensors (IMESs) for intramuscular electromyogram recording," *IEEE Trans. Biomed. Eng.*, vol. 56, no. 1, pp. 159–171, Jan. 2009, doi: 10.1109/TBME.2008.2005942.

[11] D. Farina et al., "Toward higher-performance bionic limbs for wider clinical use," *Nature Biomed. Eng.*, vol. 7, no. 4, pp. 473–485, 2023, doi: 10.1038/s41551-021-00732-x.

[12] R. E. Reilly, "An implantable EMG sensor," *Adv. External Control Hum. Extremities*, vol. 3, pp. 535–543, 1970.

[13] D. M. Pham and S. M. Aziz, "A real-time localization system for an endoscopic capsule using magnetic sensors," *Sensors*, vol. 14, no. 11, pp. 20910–20929, 2014, doi: 10.3390/s141120910.

[14] E. J. Rouse et al., "Development of a model osseomagnetic link for intuitive rotational control of upperlimb prostheses," *IEEE Trans. Neural Syst. Rehabil. Eng.*, vol. 19, no. 2, pp. 213–220, Apr. 2011, doi: 10.1109/TNSRE.2010.2102365.

[15] M. Gherardini et al., "The myokinetic interface: Implanting permanent magnets to restore the sensory-motor control loop in amputees," *Curr. Opin. Biomed. Eng.*, vol. 27, Apr. 2023, Art. no. 100460, doi: 10.1016/J.COBME.2023.100460.

[16] S. P. Mendez et al., "Data-driven real-time magnetic tracking applied to myokinetic interfaces," *IEEE Trans. Biomed. Circuits Syst.*, vol. 16, no. 2, pp. 266–274, Apr. 2022, doi: 10.1109/TBCAS.2022.3161133.

[17] A. Prakash et al., "Magnetic-based detection of muscular contraction for controlling hand prosthesis," *Sensors Actuators A: Phys.*, vol. 344, Sep. 2022, Art. no. 113709, doi: 10.1016/j.sna.2022.113709.

[18] C. R. Taylor et al., "Magnetomicrometry," *Sci. Robot.*, vol. 6, no. 57, Aug. 2021, Art. no. 656, doi: 10.1126/scirobotics.abg0656.

[19] A. Moradi et al., "Clinical implementation of a bionic hand controlled with kineticomyographic signals," *Sci. Rep.*, vol. 12, no. 1, Aug. 2022, Art. no. 14805, doi: 10.1038/s41598-022-19128-1.

[20] C. R. Taylor et al., "Untethered muscle tracking using magnetomicrometry," *Front. Bioeng. Biotechnol.*, vol. 10, Oct. 2022, Art. no. 1979, doi: 10.3389/FBIOE.2022.1010275/BIBTEX.

[21] V. Biancalana et al., "Fast, cheap, and scalable magnetic tracker with an array of magnetoresistors," *Instruments*, vol. 5, no. 1, Sep. 2020, Art. no. 3, doi: 10.3390/instruments5010003.

[22] F. Clemente et al., "Development of an embedded myokinetic prosthetic hand controller," *Sensors*, vol. 19, no. 14, Jul. 2019, Art. no. 3137, doi: 10.3390/s19143137.

[23] V. Ianniciello et al., "Myokinetic prosthesis control oriented environmental magnetic disturb analysis," in *Proc. MEC20 Symp.*, 2020.

[24] G. Shao et al., "A novel passive magnetic localization wearable system for wireless capsule endoscopy," *IEEE Sensors J.*, vol. 19, no. 9, pp. 3462–3472, May 2019, doi: 10.1109/JSEN.2019.2894386.

[25] S. Tarantino et al., "Feasibility of tracking multiple implanted magnets with a myokinetic control interface: Simulation and experimental evidence based on the point dipole model," *IEEE Trans. Biomed. Eng.*, vol. 67, no. 5, pp. 1282–1292, May 2020, doi: 10.1109/TBME.2019.2935229.

[26] C. Hu, M. Q. Meng, and M. Mandal, "Efficient magnetic localization and orientation technique for capsule endoscopy," in *Proc. IEEE/RSJ Int. Conf. Intell. Robots Syst.*, 2005, pp. 628–633, doi: 10.1109/IROS.2005.1545490.

[27] M. Gherardini et al., "Localization accuracy of multiple magnets in a myokinetic control interface," *Sci. Rep.*, vol. 11, no. 1, Dec. 2021, Art. no. 4850, doi: 10.1038/s41598-021-84390-8.

[28] F. Masiero et al., "Effects of sensor resolution and localization rate on the performance of a myokinetic control interface," *IEEE Sensors J.*, vol. 21, no. 20, pp. 22603–22611, Oct. 2021, doi: 10.1109/JSEN.2021.3109870.

[29] C. Hager-Ross and M. H. Schieber, "Quantifying the independence of human finger movements: Comparisons of digits, hands, and movement frequencies," *J. Neurosci.*, vol. 20, no. 22, pp. 8542–8550, Nov. 2000, doi: 10.1523/JNEUROSCI.20-22-08542.2000.

[30] K. C. Engel, M. Flanders, and J. F. Soechting, "Anticipatory and sequential motor control in piano playing," *Exp. Brain Res.*, vol. 113, no. 2, pp. 189–199, 1997, doi: 10.1007/BF02450317/METRICS.

[31] C. C. Norkin and D. J. White, *Measurement of Joint Motion: A Guide to Goniometry*. Philadelphia, PA, USA: FA Davis, 1985, doi: 10.2310/6640.2004.00031.

[32] T. Greiner, *Hand Anthropometry of US Army Personnel*. Natick, MA, USA: US Army Natick Res., Develop. & Eng. Center, 1991.

[33] S. Milici et al., "The myokinetic control interface: How many magnets can be implanted in an amputated forearm? Evidence from a simulated environment," *IEEE Trans. Neural Syst. Rehabil. Eng.*, vol. 28, no. 11, pp. 2451–2458, Nov. 2020, doi: 10.1109/TNSRE.2020.3024960.

[34] M. Gherardini, A. Mannini, and C. Cipriani, "Optimal spatial sensor design for magnetic tracking in a myokinetic control interface," *Comput. Methods Prog. Biomed.*, vol. 211, Nov. 2021, Art. no. 106407, doi: 10.1016/j.cmpb.2021.106407.

[35] F. Paggetti et al., "To what extent implanting single vs pairs of magnets per muscle affect the localization accuracy of the myokinetic control interface? Evidence from a simulated environment," *Trans. Biomed. Eng.*, vol. 70, no. 10, pp. 2972–2979, Oct. 2023, doi: 10.1109/TBME.2023.3272977.

[36] T. R. Farrell and R. F. Weir, "The optimal controller delay for myoelectric prostheses," *IEEE Trans. Neural Syst. Rehabil. Eng.*, vol. 15, no. 1, pp. 111–118, Mar. 2007, doi: 10.1109/TNSRE.2007.891391.

[37] L. H. Smith et al., "Determining the optimal window length for pattern recognition-based myoelectric control: Balancing the competing effects of classification error and controller delay," *IEEE Trans. Neural Syst. Rehabil. Eng.*, vol. 19, no. 2, pp. 186–192, Apr. 2011, doi: 10.1109/TNSRE.2010.2100828.

[38] K. S. Oh and D. M. Kim, "Rechargeable lithium ion battery model : INR18650 MJ1 3500mAh," LG Chem, 2014. [Online]. Available: http://www.lgchem.com

[39] E. Mastinu et al., "Embedded system for prosthetic control using implanted neuromuscular interfaces accessed via an osseointegrated implant," *IEEE Trans. Biomed. Circuits Syst.*, vol. 11, no. 4, pp. 867–877, Aug. 2017, doi: 10.1109/TBCAS.2017.2694710.

[40] S. Benatti et al., "A versatile embedded platform for EMG acquisition and gesture recognition," *IEEE Trans. Biomed. Circuits Syst.*, vol. 9, no. 5, pp. 620–630, Oct. 2015, doi: 10.1109/TBCAS.2015.2476555.

[41] G. A. Demichele et al., "Low-power polling mode of the next-generation IMES2 Implantable wireless EMG sensor," in *Proc. IEEE 36th Annu. Int. Conf. Eng. Med. Biol. Soc.*, 2014, pp. 3081–3084, doi: 10.1109/EMBC.2014.6944274.

Open Access provided by 'Scuola Superiore "S.Anna" di Studi Universitari e di Perfezionamento' within the CRUI CARE Agreement